Terr. Atmos. Ocean. Sci., Vol. 24, No. 3, 295-310, June 2013 doi: 10.3319/TAO.2013.01.10.01(T)

A Two-Dimensional Post-Stack Seismic Inversion for Acoustic Impedance of Gas and Hydrate Bearing Deep-Water Sediments Within the Continental Slope of the Ulleung Basin, East Sea, Korea

Keumsuk Lee[1], Dong-Geun Yoo[2, *], George A. McMechan[3], Namsoon Hwang[4], and Gwang H. Lee[5]

[1] *Korea National Oil Corporation, Anyang, Korea*
[2] *Petroleum and Marine Research Division, Korea Institute of Geoscience and Mineral Resources (KIGAM), Daejon, Korea*
[3] *Center for Lithospheric Studies, University of Texas at Dallas, Dallas, Texas, USA*
[4] *Department of Energy Technology, University of Science and Technology, Daejeon, Korea*
[5] *Department of Energy Resources Engineering, Pukyong National University, Busan, Korea*

Received 20 April 2012, accepted 10 January 2013

ABSTRACT

A post-stack inversion of 2D seismic data was conducted to estimate the spatial distribution of acoustic impedance associated with gas and hydrates in the Ulleung Basin, East Sea, Korea constrained by logs from three boreholes drilled on its continental margin. A model-based inversion was applied to a Plio-Quaternary succession composed of alternations of unconsolidated mass-flow deposits/turbidites. A comparison of seismic reflections and synthetic data computed from impedance logs is shown for two zones. An upper (steep) slope zone contains a moderately continuous, possibly bottom-simulating reflector feature along the corresponding section. This feature may be associated with a lithology boundary near a drill site in addition to, or instead of, a stability boundary of gas hydrates (i.e., gas below and hydrates above). The lower (gentle) slope zone has locally cross-cutting reflection patterns that are more likely to be attributed to gas- and hydrate-related physical phenomena than to spatiotemporal changes in lithology. This seismic inversion is informative and useful, making a contribution to enhance the interpretability of the seismic profiles for a potential hydrate recovery.

Key words: Post-stack acoustic inversion, Seismic chimney, Gas hydrate, BSR

Citation: Lee, K., D. G. Yoo, G. A. McMechan, N. Hwang, and G. H. Lee, 2013: A two-dimensional post-stack seismic inversion for acoustic impedance of gas and hydrate bearing deep-water sediments within the continental slope of the Ulleung Basin, East Sea, Korea. Terr. Atmos. Ocean. Sci., 24, 295-310, doi: 10.3319/TAO.2013.01.10.01(T)

1. INTRODUCTION

Gas hydrates are crystalline solids containing gas molecules, usually methane, entrapped within a rigid cage of water molecules. Methane hydrates are stable under conditions of low temperature and high pressure (Hyndman and Davis 1992), requiring the ice-like mixtures to be usually confined to the upper few hundred meters (< 300 m) of the sediment column along the continental margins. The depth extent of their occurrence is defined by the gas-hydrate stability zone (GHSZ) and is constrained by the interaction of the geothermal gradient, water column-related parameters (e.g., bottom-water temperature, pressure), gas composition, chlorinity, and the physical and chemical properties of the gas-hydrate bearing sediments (Dickens and Quinby-Hunt 1997).

The maximum depth of the GHSZ is a phase boundary between the lower limit of gas-hydrate stability and the possible upper limit of free gas; thus, the corresponding seismic reflection has reverse polarity to that of the seafloor. This may be clearly observed in seismic profiles (if there is a sufficiently strong acoustic impedance contrast), where it parallels the seafloor and typically cuts across stratigraphic boundaries. It is referred to as a bottom simulating reflection (BSR) (Shipley et al. 1979).

Gas chimneys with their associated seismic acoustic attenuated zones are gas and/or gas hydrate-related indicators in the reflection data. High-amplitude reflections and/or acoustic turbidity tend to disappear gradually or become weaker near the base of the GHSZ (Horozal et al. 2009;

* *Corresponding author*
E-mail: dgyoo@kigam.re.kr

Netzeband et al. 2010). The related seismic anomalies commonly occur beneath concave or convex seafloor expressions on seismic profiles (Ginsburg 1998); these zones are considered to be vertical conduits for fluids, probably migrating from below the GHSZ (Hyndman et al. 2001; Wood et al. 2002).

Since the early 2000s, seismic indicators of gas and gas-hydrates have been observed in 2D/3D seismic reflection data acquired in numerous places in the Ulleung basin. These indicators include BSRs, acoustic anomalies (e.g., reflections with enhanced low-frequency below the BSR), and gas chimneys. As a result of extensive exploration activities, methane hydrates were successfully recovered from two of the five wells that were drilled in the deep-sea basin in 2007.

Since the 1970s, post-stack acoustic seismic inversion has been a widely used technique in the petroleum industry for subsurface geological inferences (e.g., lithology, porosity) based on seismic analysis tied to well logs (i.e., resistivity, sonic and density). The method increasingly confirms the usefulness of inverted seismic data and is informative for seismic interpretation (Buiting and Bacon 1999). Post-stack inversion produces only P-impedance output as it uses normal incidence reflections and requires only near-offset stack data (rather than full aperture stacked data) to obtain physically and geologically reliable results. The method is more commonly applied to conventional oil and gas reservoirs, but there are a few papers (e.g., Lu and McMechan 2002; Inamori and Hato 2004; Bellefleur et al. 2006) that document applications of seismic acoustic inversion to the characterization of gas-hydrate bearing deep-sea sediments.

This paper presents an application of model-based post-stack seismic inversion to estimate acoustic impedance and its variations associated with the Plio-Quaternary gas and hydrate-bearing lithology in the Ulleung Basin. The acoustic impedance is inverted from near-offset (multi-channel) seismic reflection data collected in 2005 with constraints from logging-while-drilling (LWD) results and cored samples from a drilling program launched by KIGAM (Korea Institute of Geoscience and Mineral Resources) in 2007. The approach in the present study is to demonstrate that inversion of seismic data from the gas- and hydrate-bearing deep-water sediments is a useful tool for seismic interpretation, especially when integrated with and constrained by borehole data.

2. GEOLOGICAL SETTING

The Ulleung Basin is part of a Tertiary back-arc system that is bordered to the north by the Japan basin and to the east by the Yamato basin forming the East Sea (Fig. 1). The

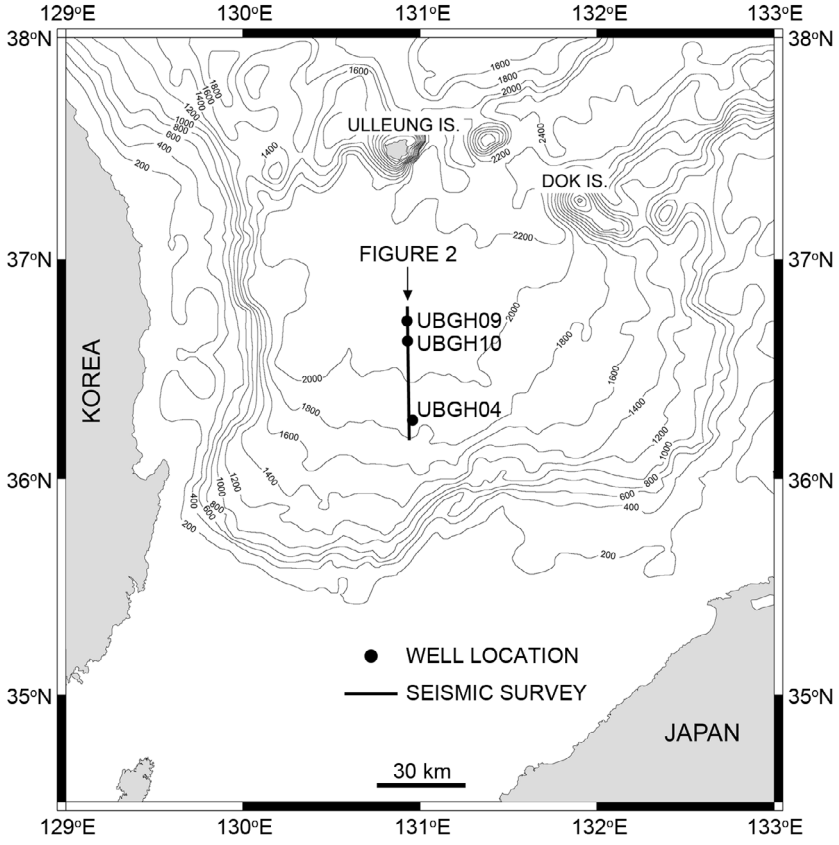

Fig. 1. Bathymetry of the Ulleung Basin and location map with drilling sites selected for hydrate recovery.

deep back-arc basins were developed commencing from the early Oligocene (Tamaki et al. 1992) through the late Miocene (Tamaki and Honza 1985) between the Precambrian-Paleozoic craton of the Korean Peninsula to the west and the Cenozoic Japanese Island arc to the east.

The Tertiary basin appears to be sourced either from its southern uplifted continental margin during the evolution of the East Sea (Yoon et al. 2003) or from large-scale slope failures likely triggered by earthquakes (Lee et al. 1996). The resulting turbidites and mass-flows transported sediments into the deepwater setting. As a result, the deep-sea basin is filled with stacked mass-flow deposits associated, and/or alternating with, possibly organic-rich turbidites/hemipelagic sediments (THS), which appear to be related to the occurrence of gas chimneys near the center of the basin (Figs. 2 and 3).

The basin also appears to provide favorable conditions for gas and gas hydrates which are recognized as BSRs on the multi-channel seismic data. The BSR in the seismic data (Fig. 2) has four salient characteristics: (1) It is parallel to the seafloor reflection; (2) It has polarity opposite to the seafloor reflection; (3) It generally cuts across the lithologic

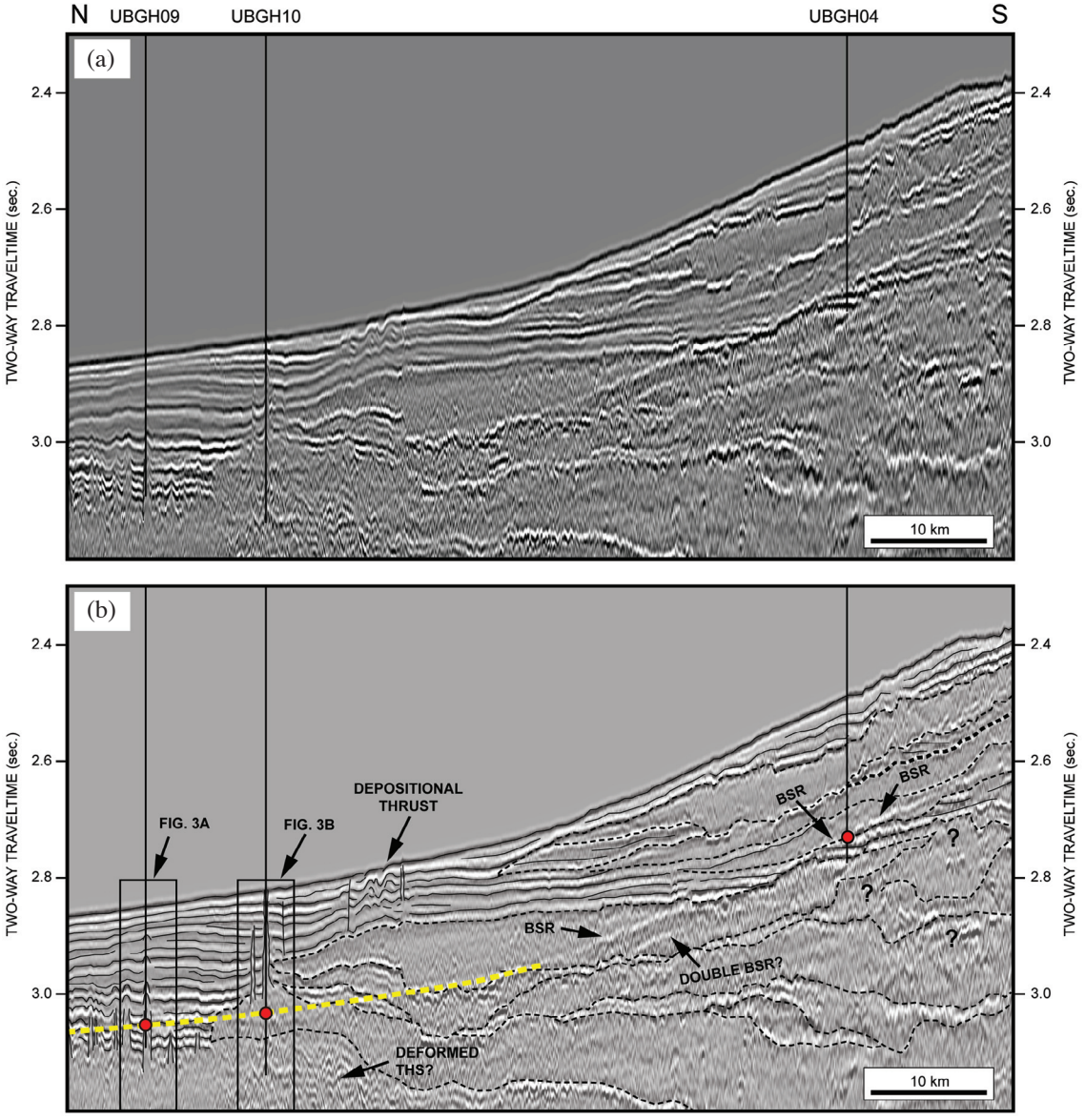

Fig. 2. Un-interpreted (a) and interpreted (b) seismic profiles across the lower continental slope containing BSRs in the shallower region and gas chimneys in the deeper region. UBGH04, 09 and 10 are borehole sites (see Fig. 1 for location). Dashed solid and thin lines are the interpreted geometry of mass-flow deposits corresponding to seismic facies 1 (SF1), and thin lines bound turbidite/hemipelagic sediments (THS) corresponding to seismic facies 2 (SF2), respectively (see Fig. 3 for details). The vertical solid lines indicate the vertical extent of the three boreholes. The red, open circles represent the bottom of the GHSZ computed from the in-situ measurements at the borehole sites (see Table 2 for parameters) and the dashed yellow line is the base of the GHSZ predicted by interpretation of the seismic data.

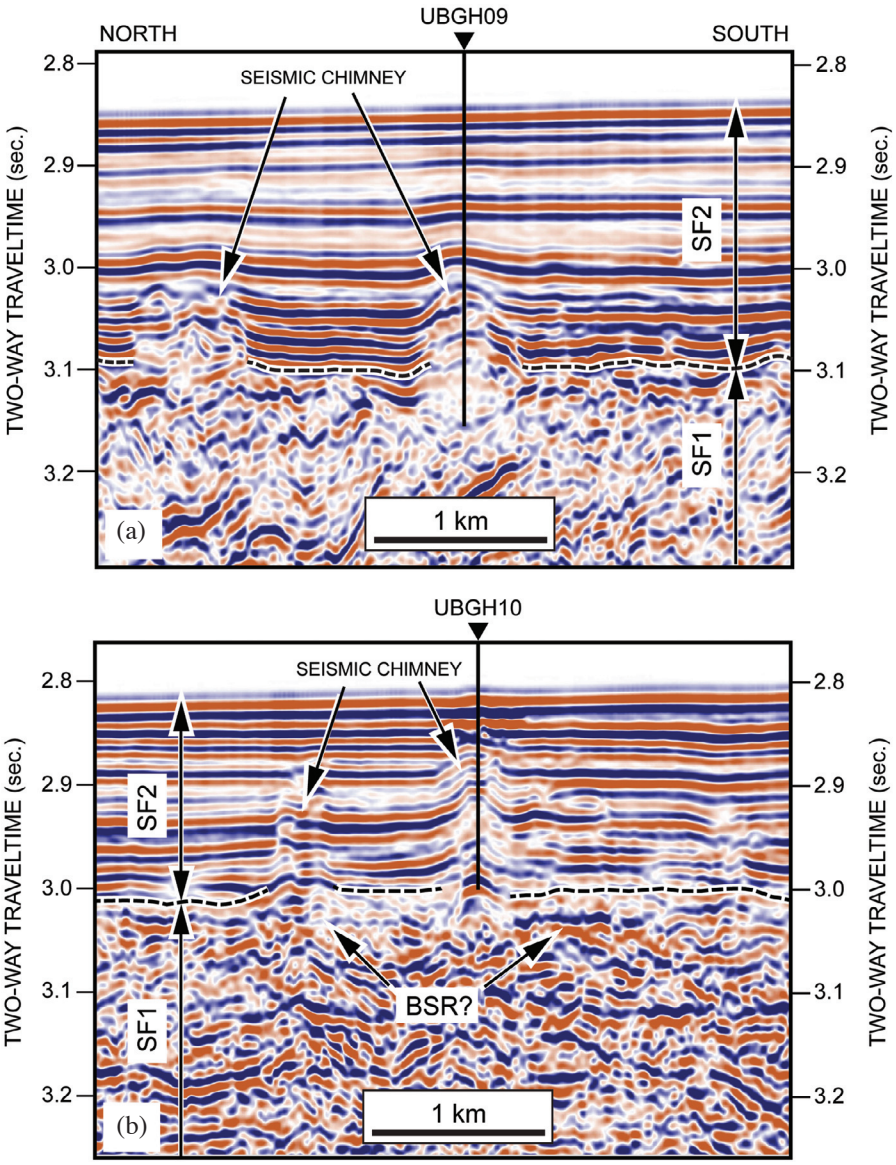

Fig. 3. Seismic profiles associated with UBGH09 (a) and 10 (b) showing the detailed SF1 and SF2 which are bounded by dashed lines (see Fig. 2 for location).

boundaries, indicating that it is a physical rather than a sedimentological boundary; and, (4) its position is consistent with that predicted by thermodynamic correlation, as determined below. Their existence is confirmed by methane hydrate recovery from about 150 mbsf (meters below the sea floor) at a water depth between 1800 and 2100 m (Park et al. 2008). Sometimes the seismic profiles show possible double BSRs, with a faint second BSR occurring below the main ones in the mass-flow deposits (e.g., Figs. 2 and 3). The lower BSR may be a remnant BSR produced by a climate-driven shift of the stability zone for gas and hydrates (Popescu et al. 2006), or a shift caused by a change in water depth produced by a rapid increase in sediment thickness accumulated by a new mass-flow deposit, or the presence of two or more hydrates associated with gases of differing chemistry and therefore different stability depths (Andreassen et al. 2000).

3. SUBSURFACE DATABASE

The database used in the present study includes seismic data, well logs and cored samples. A total of 6600 km of 2D high-resolution, multi-channel seismic reflection data were acquired on a grid of 4 km × 4 km line spacings running north-south and east-west. The collected seismic data were re-sampled at 2 ms and zero-phased before stacking and time-migration. The present study uses one of the seismic profiles (Fig. 2a) recorded in the north-south direction

across three wells (UBGH04, 09 and 10) (Fig. 1); for these data, the source and receiver increments are 25 and 12.5 m, respectively The minimum and maximum offsets are 160 and 3147.5 m, respectively.

Prior to the Kirchhoff pre-stack time migration, the input section was filtered with a zero-phase time-variant filter. The filter pass bands were set with low-(3 Hz) and high-cut frequencies (110 to 40 Hz for 2000 to 6000 ms, respectively) to optimize the removal of high frequency noise by having the filter following the noise spectrum as a function of time. After the normal move-out (NMO) correction, the traces in the shot gathers were separated into ranges of incident angles. The near-angle stack (0 - 15 degrees) was extracted for the present study.

Three locations of predicted gas-hydrate occurrences were drilled and cored to a depth of about 220 mbsf. The hole UBGH04, which is located about 820 m off the seismic line, was drilled into the upper slope BSR (Fig. 2b). Holes UBGH09 and UBGH10, which are located very close to the seismic line, penetrate the low-angle seafloor and target seismic chimney features (Fig. 3). The UBGH04 location was selected on the basis of a 3D seismic volume acquired for a detailed site survey after the BSR was identified on the seismic profile. The corresponding three holes were logged with logging-while-drilling (LWD) tools measuring natural gamma, relative resistivity, relative density, relative neutron porosity, and sonic velocity (Figs. 4, 5 and 6). The gas compositions of the pore space of the cored samples were analyzed to measure the amount of chlorinity and gas compositions in the seawater (Fig. 6).

The core recovery for all boreholes is greater than 40%. Because the cored samples are unconsolidated sediments, it is difficult to determine a detailed distribution of grain size. The sedimentary samples of the UBGH04 well consist of silt (80%), clay (10%) and sand (10%) which increase abruptly over two intervals: 60 - 65 mbsf (80%)

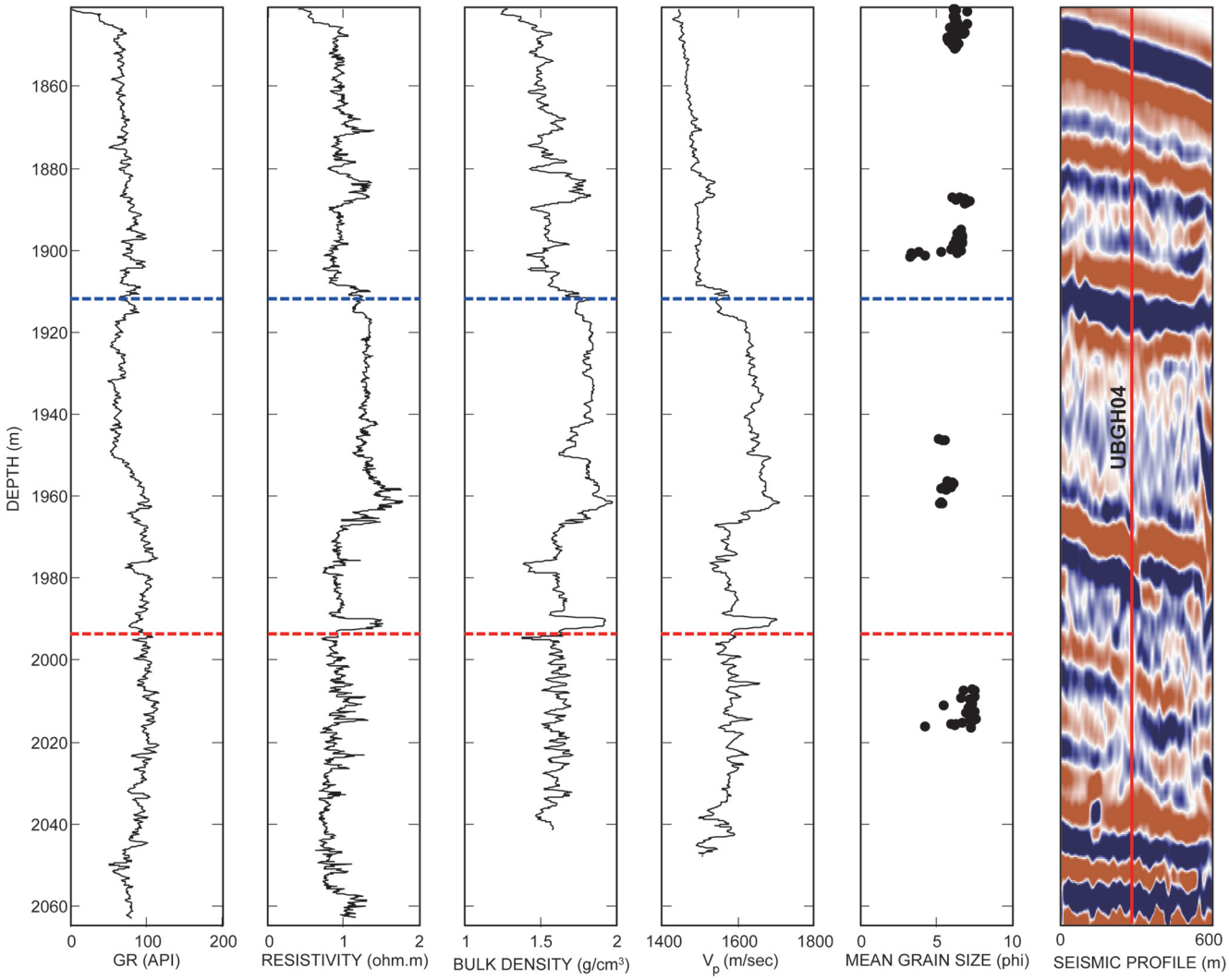

Fig. 4. Downhole logs and corresponding seismic data from the UBGH04 well. The seafloor is at 1841.4 m. Mean grain size is modified from KIGAM (2008). The red and blue dashed lines indicate a predicted BSR (See Table 1) and a possible top of hydrate, respectively.

and 170 - 180 mbsf (40%) (Fig. 4). The UBGH09 and 10 wells show a similar variation in grain size to that in the UBGH04 well but these are different in variation of sand increasing from 20% at the top to 90% at about 125 mbsf (Fig. 5) and from 20% to 60% for the entire section (Fig. 6), respectively.

Fugro-McClelland (2008) reported that the geophysical data and gas analysis on the non-pressurized cores show the possibility of gas hydrates at the sites (Fig. 7). The predicted gas hydrate concentration in UBGH04 is about 44%, in relatively coarse grained (silty-sandy) samples at about 185 mbsf; no hydrates were observed in the core samples.

However, the two other cores (UBGH09 and 10) contain solid gas hydrates (Kang et al. 2009) (Table 1) with a dominant methane composition. The gas-hydrate bearing sediments in UBGH09 are silty and/or sandy layers between 63 and 151 mbsf, within which intervals contain an average pore volume fraction of hydrates of 30%, reaching a maximum of 64%. Hole UBGH10 shows a fluctuating chlorinity down to 100 mbsf, indicative of possible recent hydrate formation. The predicted hydrate saturation in the sediments of UBGH10 is substantially lower than that of UBGH09, dropping down to about 1.4% of sediment volume above the predicted BSR. The marked top of hydrate in UBGH10 indicated by a blue dashed line in Fig. 6 is anomalously shallow because of the distortion of the GHSZ by the gas chimney that the hole penetrates.

4. SEISMIC SIGNATURES

The seismic data contain two distinct facies: seismic facies 1 (SF1) and 2 (SF2) (Fig. 3). SF1 is characterized by discontinuous, chaotic low-amplitude reflections, whereas SF2 is characterized by relatively well-defined conformable reflections. The disturbed seismic facies forming an elongate unit is interpreted as mass-flow deposits that are verti-

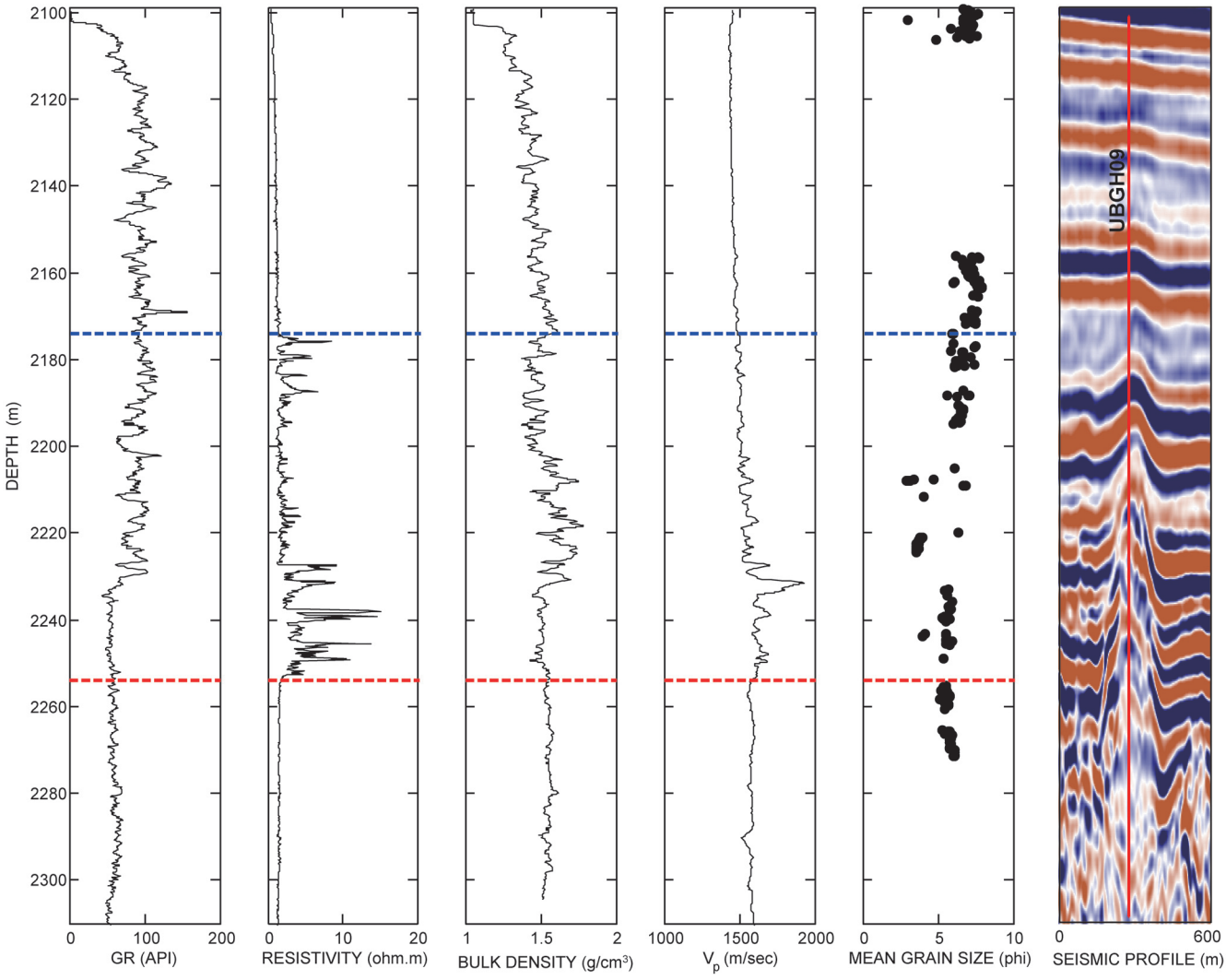

Fig. 5. Downhole logs and corresponding seismic data from the UBGH09 well. The seafloor is at 2099.1 m. Mean grain size is modified from KIGAM (2008). The red and blue dashed lines indicate a predicted BSR (See Table 1) and a possible top of hydrate, respectively.

cally and/or laterally associated with continuous reflection patterns (SF2) which is interpreted as THS (e.g., Horozal et al. 2009). The basal surface of the SF1 includes a combination of linear scour marks and a side-wall scarp; and, its top forms a relatively rugose surface that is either filled and draped by concordant strata (SF2) or becomes the base of the overlying new SF1s.

The Plio-Quarternary section appears to be dominated by SF1 that exists in the form of a vertically and laterally stacked geometry over much of the slope area with different sizes and shapes. The various geomorphologies of the disturbed seismic reflectors indicate that the high-energy deep-water process related to a transformation of a mass flow to a Newtonian turbidity current (Shanmugam 2006) occurred numerous times in various directions during the Tertiary period and that it removed whole or partial pre-existing turbidites or old mass-flow deposits (which may be or may not be seen here). A relatively heavy sediment load accompanying the mass-flow deposits may cause syn-depositional thrusts as indicated by locally differently folded internal reflections of SF2 (Fig. 2b).

At UBGH04, the two distinct seismic textures on the profile correspond to increase in resistivity, density and P-wave velocity in the LWD data (Fig. 4) and are consistent with general physical characteristics of high-energy induced deep-water deposition (e.g., Shipp et al. 2004). However, the local vertically disturbed seismic features around both UBGH09 and 10 appear to be relevant to the existence of gas and hydrates as described below.

5. CALCULATION OF GHSZ THICKNESS

A possible depth to the bottom of a GHSZ in the marine environment may be predicted by a computation on the basis of the in-situ seafloor temperature and geothermal equations developed by Miles (1995) for the gas hydrate

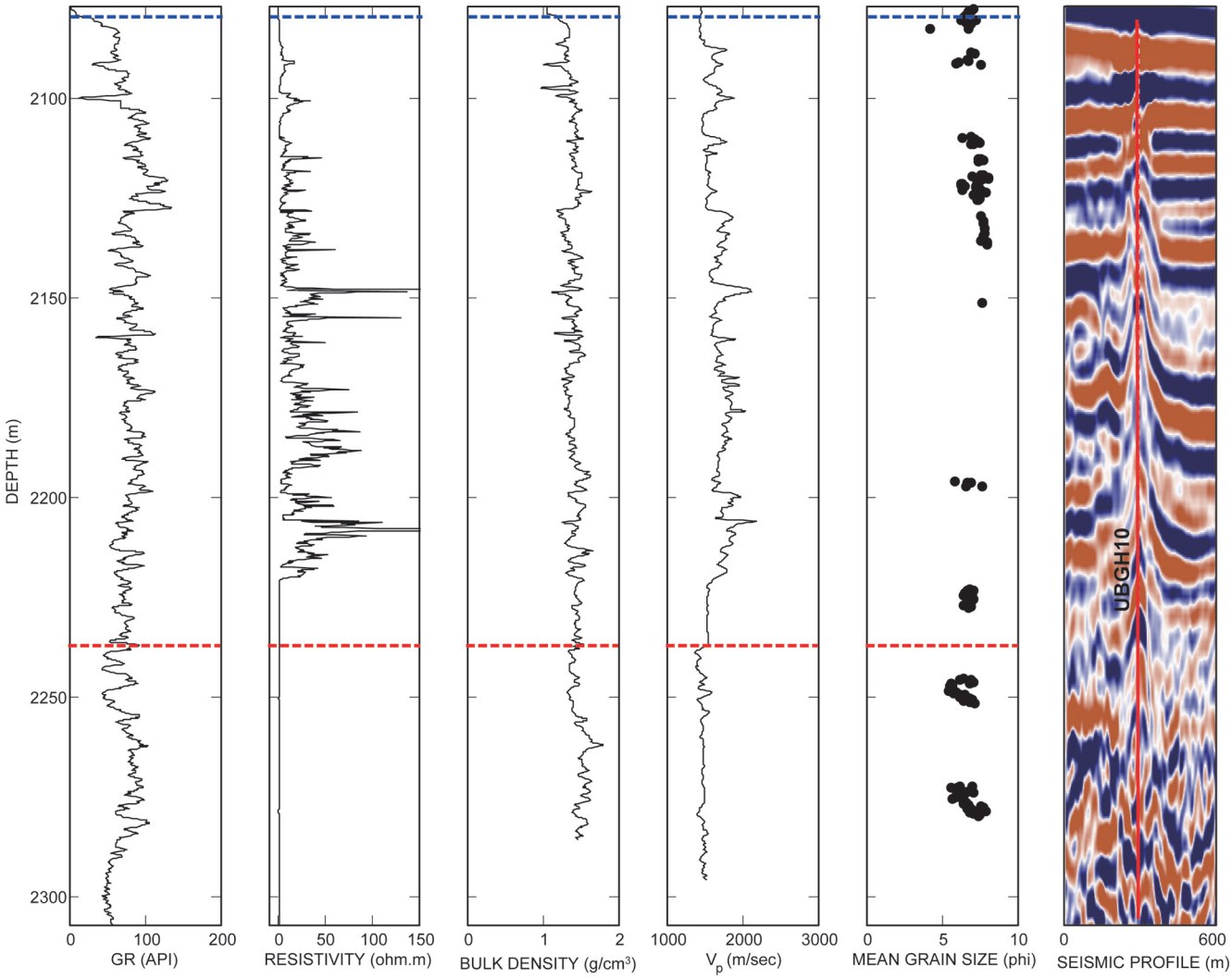

Fig. 6. Downhole logs and corresponding seismic data from the UBGH10. The seafloor is at 2077 m. Mean grain size is modified from KIGAM (2008). The red and blue dashed lines indicate a predicted BSR (See Table 1) and a possible top of hydrate, respectively.

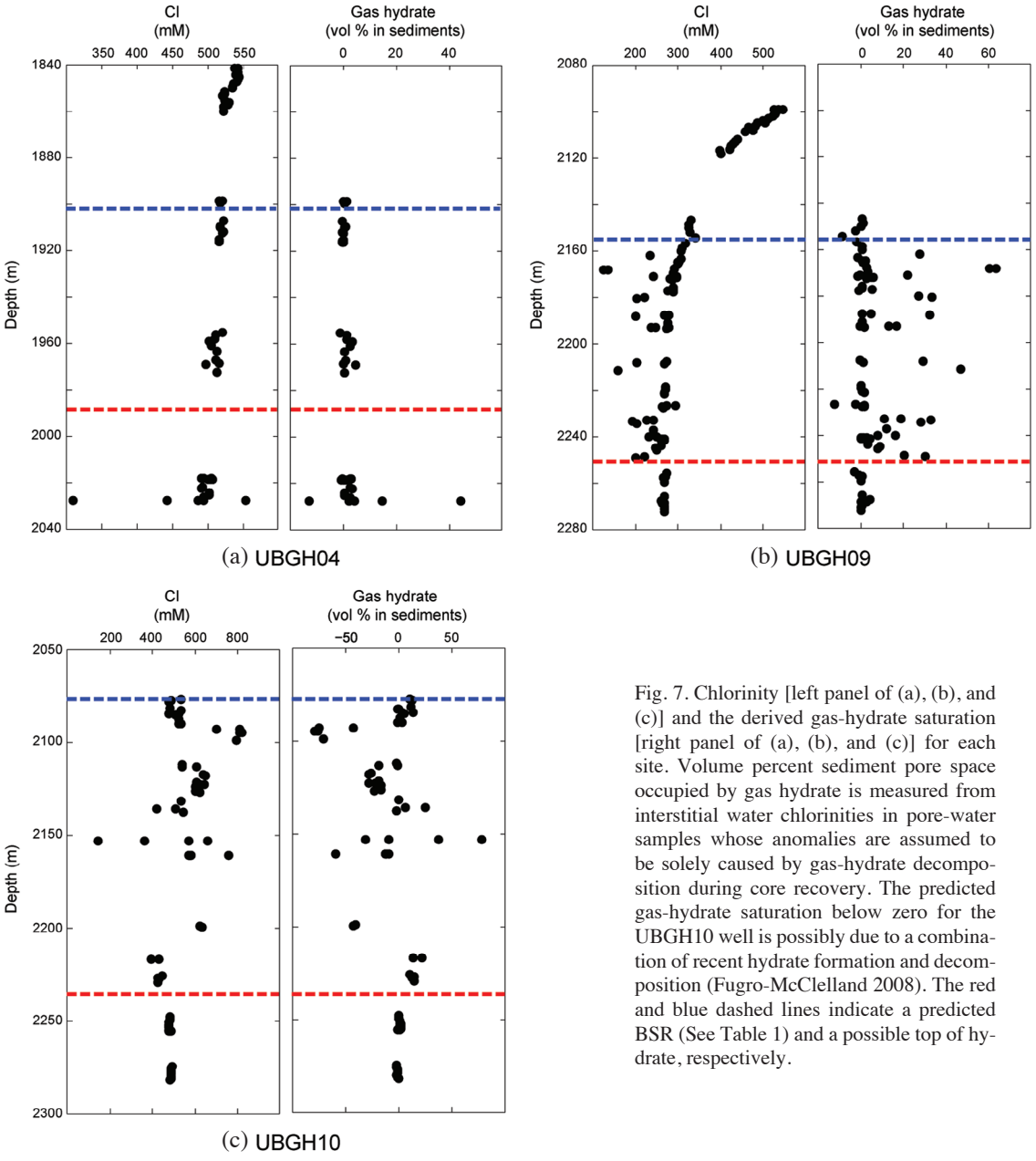

Fig. 7. Chlorinity [left panel of (a), (b), and (c)] and the derived gas-hydrate saturation [right panel of (a), (b), and (c)] for each site. Volume percent sediment pore space occupied by gas hydrate is measured from interstitial water chlorinities in pore-water samples whose anomalies are assumed to be solely caused by gas-hydrate decomposition during core recovery. The predicted gas-hydrate saturation below zero for the UBGH10 well is possibly due to a combination of recent hydrate formation and decomposition (Fugro-McClelland 2008). The red and blue dashed lines indicate a predicted BSR (See Table 1) and a possible top of hydrate, respectively.

Table 1. A list of hydrates observed in the cores from the UBGH09 and 10 wells. The hydrates are within the predicted zones as in Fig. 2.

Sample No.	Depth of Sample (mbsf)	Well Name	Occurrence	Sample No.	Depth of Sample (mbsf)	Well Name	Occurrence
1	15.00	UBGH10	Veins in mud	9	77.22	UBGH10	Nodules and veins in mud
2	18.15	UBGH10	Nodules and veins in mud	10	110.00	UBGH10	Nodules and veins in mud
3	22.60	UBGH10	Nodules and veins in mud	11	140.00	UBGH10	Nodules and veins in mud
4	22.87	UBGH10	Nodules in mud	12	140.65	UBGH10	Nodules and veins in mud
5	35.50	UBGH10	Nodules and veins in mud	13	141.00	UBGH10	Veins in mud
6	41.16	UBGH10	Nodules in cemented sand	14	70.55	UBGH09	Nodules and veins in mud
7	61.86	UBGH10	Nodules and veins in mud	15	120.00	UBGH09	Nodules in cemented sand
8	76.00	UBGH10	Nodules and veins in mud				

phase equilibrium diagrams. On the basis of the phase equilibrium relation, Rao (1999) provides a detailed description of GHSZ thickness calculation. During the drilling campaign, the seabed temperature and geothermal gradient were measured at all the well locations in the Ulleung Basin including the UBGHs (Table 2). This alternative prediction is useful in a seismically chaotic zone where the base of the GHSZ may be incoherent because of internal variations, erosional textures, changes in gas content, salinity, and/or heat flow. Such anomalies are consistent with the presence of gas chimneys; both UBGH09 and UBGH10 go through gas chimneys (Figs. 2b and 3). The thermally predicted locations of the BSR (the red dots) match well with the bases identified BSR from the seismic data (the yellow dashed line) in both wells (Figs. 2b and 3).

6. MODEL-BASED SEISMIC INVERSION

6.1 Overview

A model-driven process (Russell and Hampson 1991) is used to invert post-stack migrated seismic data. The main steps in the procedure include calibration by tying well logs to the seismic data, estimation of the wavelet, generation of a low-resolution background model, and inversion. The model parameterization is in two parts; blocked layers superimposed on a smoothed background (as impedance is a layer property, not an interface property). This deterministic inversion is straightforward and compares favorably with other deterministic methods (including trace integration, and sparse-spike inversion) (Veeken and Da Silva 2004). Sparse-spike inversion is limited to models with a relatively few thick layers, and trace integration assumes constant density. The specific software used in this paper is the commercial implementation called STRATA by CGGVeritas (2011).

The inversion is model-based and iterative. It is model-based in the sense that solutions are constrained to the neighborhood of a 1-D layered low-resolution background impedance model, which is derived via seismic velocity analysis, or (as in the example below), from smoothed well logs. It is iterative in the sense that the solution gradually improves the fit between synthetic traces [produced by convolution of the reflectivity impulse response (r) of the layered model with a wavelet (W)], and the observed seismic data (S).

The solution attempts to simultaneously solve for the best-fit reflectivity, and to minimize the differences between the observed S and predicted ($W * r$) seismic traces. Thus, the objective function to be minimized has two terms, corresponding to these two goals.

$$O = S - W * r \tag{1}$$

where * means convolution.

The system of linearized Eq. (1) is solved for r (and sometimes also simultaneously for W), by any iterative algorithm; the constrained conjugate gradient method (e.g., Golub and Ye 1999) is used in the examples below. The impedance (Z_i) of layer i is derived recursively from the impulse response r_j using

$$Z_i = Z_1 \prod_{j=2}^{i} \left(\frac{1 + r_j}{1 - r_j} \right) \tag{2}$$

where the impedance of the uppermost layer Z_1 needs to be input to start the recursion. Thus, Eq. (1) solves for the impulse response of the model (r) given the estimated source wavelet (W) and the synthetic seismic data ($W * r$). The model data would be different from the real data (S), because of incorrect reflectivity and noise involved. This may be resolved by minimizing the difference between the observed and synthetic data using L_2-norm optimization (Menke 1984) to obtain the best-fit layer impedances from the r sequence by Eq. (2).

The inversion algorithm used in this study constrains the impedance values to lie between upper and lower limits, which can prevent data outliers or acquisition errors from destroying the solution. Interpretation of results of model-based inversion will always be non-unique because there is an uncertainty in the relations between acoustic impedances and variations in mineral composition, pore fluids, and pore geometry. Lateral variations do occur in the estimated impedance model via interpolation and extrapolation between the constraining well logs.

Table 2. Input parameters for a computation of estimated depths of hydrate stability zone (HSZ) at the three wells.

Well Name	Longitude (Decimal)	Latitude (Decimal)	Bathymetry (m)	Seafloor Temp. (°C)	Geothermal Gradient	Base of HSZ Temp. (°C)	HSZ Depth (mbsf)
UBGH04	36.3	130.91	1841.4	0.212	0.1102	17.46	156.5
UBGH09	36.7	130.89	2099.1	0.231	0.1104	18.40	164.6
UBGH10	36.6	130.89	2077.0	0.216	0.1117	18.32	162.1

6.2 Wavelet Estimation

A source wavelet is estimated from the seismic data at each of the three holes by aligning and averaging all the reflections across groups of ten stacked traces surrounding each of the three boreholes (Fig. 8). The wavelets have a length of 200 ms and a taper of 25 ms, are zero phase, and have positive amplitude for a positive impedance contrast. The amplitude spectra of the symmetrical wavelets are computed using the autocorrelation of the input seismic traces in the frequency domain, prior to an inverse Fourier Transform to produce the wavelet which is summed with others computed from the rest of the selected traces.

The wavelet extracted for each hole is evaluated by convolving it with the impedance log of the other two holes to generate a synthetic seismic trace to tie with the recorded data traces at those holes. The wavelet predicted from the UBGH04 seismic data is modified by zeroing the samples below and above 50 ms to remove unwanted side-lobes which are attributed to a relatively uneven distribution of frequency components (Fig. 8b). Consequently, the modified wavelet (Fig. 8c) fits better across all three holes (as determined by the corresponding L_2 residual) and was chosen for input to the post-stack inversion. Only near-offset traces are included in the stack so that the amplitudes are fairly constant, generating a good approximation to a zero offset section.

6.3 Background Impedance Model

Multiplication of the relative density and sonic logs from each of the three wells produces acoustic impedance logs which correlate with a fundamental rock property (Fig. 9). The converted acoustic impedance logs are filtered (via a 15 Hz high-cut filter) to generate an initial background model for the inversion (Fig. 10a). The smoothed well logs are interpolated between and beyond the holes guided by control horizons picked from the seismic profile in a 350 - 400 ms window that starts at the sea floor and extends slightly deeper than the bottom of the wells (Fig. 10a).

The impedance variations of all boreholes are constrained to lie between the lower (1483 m s^{-1} × g cc^{-1}) and upper (3389 m s^{-1} × g cc^{-1}) values (Fig. 9). Ten initial models were recursively iterated with processing sampling rate of 2 ms to predict the optimized acoustic logs and thus synthetic seismic data. The correlation coefficient and the percent difference between predicted data and the real seismic traces average 0.99, and 0.14, respectively (Fig. 9). The well-matched logs are also interpolated throughout the input seismic profile guided by control horizons (Russell and Hampson 1991) whereby a 2D inversion is constructed.

The result is a 2D section containing the estimated low-resolution acoustic impedance (Fig. 10a). As a consequence of lateral sedimentological facies variations along the southern slope of the basin, the original UBGH04 impedance log

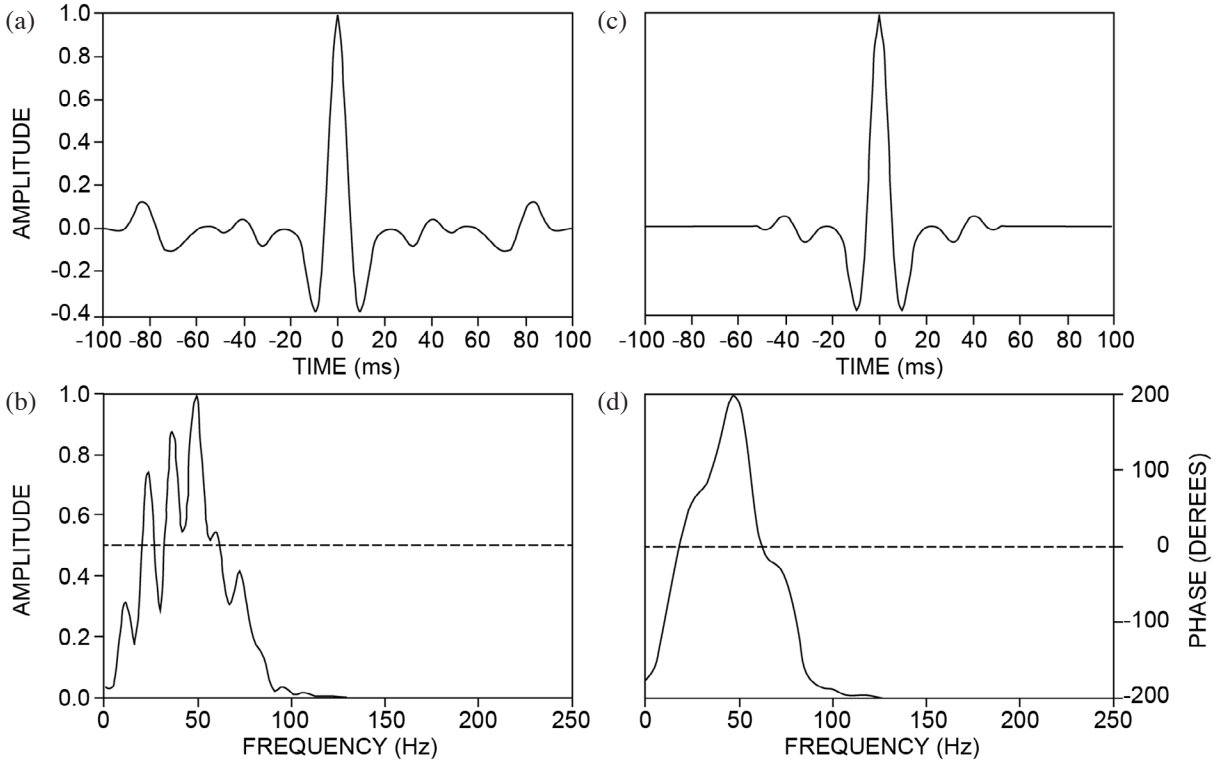

Fig. 8. The zero-phased wavelet (a) and the corresponding frequency spectrum (b) derived at the UBGH04 site. The modified wavelet (c) and the corresponding frequency spectrum (d) applied at the other sites (UBGH09 and 10) prior to the seismic inversion.

(and also its smoothed version) shows notable impedance variations. The anomalous impedance behavior at UBGH09 and 10 is caused by the inferred occurrence of gas chimneys in the sediments (Figs. 3, 5 and 6).

The predefined low-resolution background impedance section (Fig. 10a) extends the seismic bandwidth by being added to the high-frequency impedance variations that are output by the impedance inversion in the next section. Visual comparison of the real seismic data and that predicted by the impedance logs and the estimated source wavelet at the holes (Fig. 9) shows a good correlation. This gives confidence that the impedances produced by the inversion for the inter-hole regions will be of similar high quality, and geologically realistic.

7. INVERSION RESULTS

7.1 Description

Impedance gives more salient information on rock properties than amplitudes, and it is represented in the form of a layered model. The P-impedance inversion uses a zero-offset section, or a near-angle stack, as input. The near-angle stack has relative amplitudes similar to those at zero-offset, but the summed seismic data have the advantage of improved S/N ratio compared to zero offset alone. Amplitudes near the zero offset usually change slowly, are not affected by P-to-S conversion, and can be considered to be reliable.

The wavelet and background impedance model calibrated at the boreholes are input to inversion of the near-angle stacked data. The resulting post-stack seismic inversion shows geologically consistent impedance along the depositional dip section through the three drill sites (Fig. 10b). The acoustic impedance values from the borehole logs are well matched with those in the inverted seismic data as expected from the correlation between the extracted source wavelet at all the three holes; the high impedance zone agrees well with the high velocity part of the logs (Fig. 9).

There are large lateral and vertical variations in the inverted acoustic impedance along the seismic profile (Fig. 10b). The relatively high seismic impedance progressively decreases downward forming a laterally continuous geometry with varying thickness of sediments (Fig. 10b). The up-dip slope part of the section is characterized by two high-impedance (i.e., high density and velocity) zones: the upper one (UIZ1 in Fig. 11a) is thicker (up to 80 ms) and a higher continuity than the lower zone (UIZ2 in Fig. 11a). The impedance contrast at the BSR becomes weak and

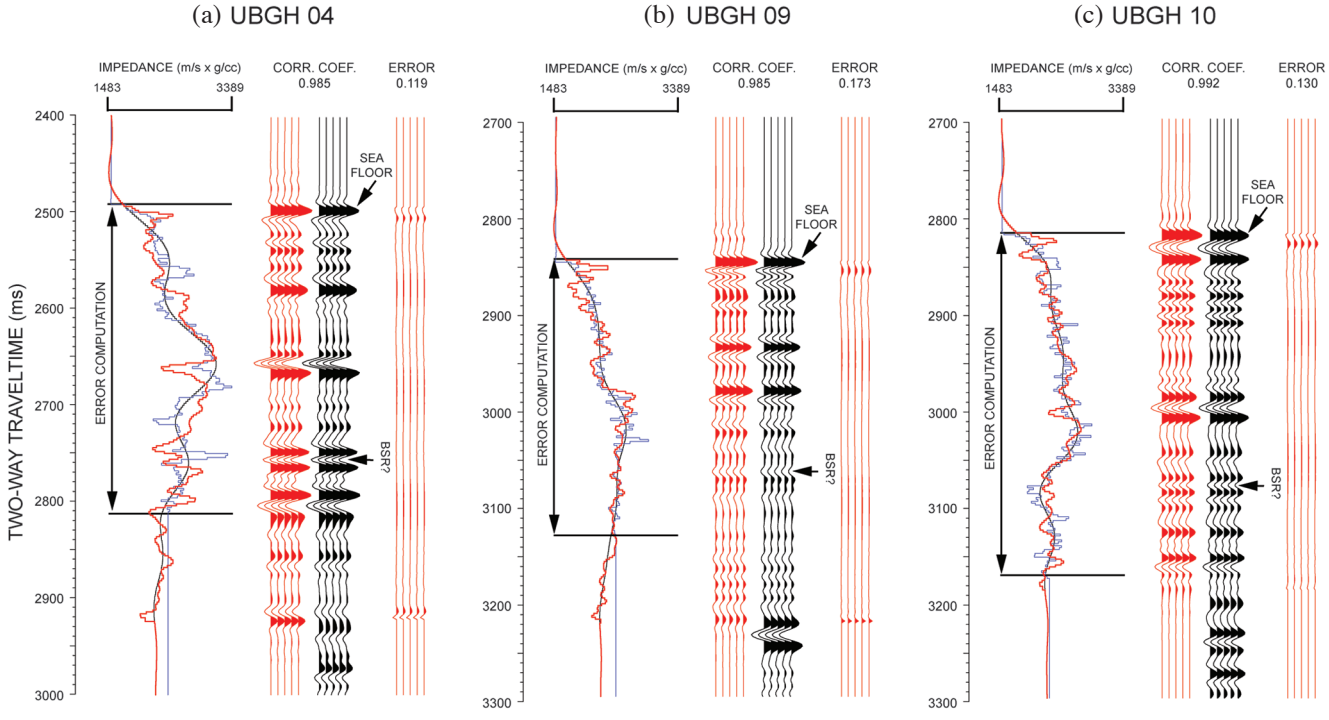

Fig. 9. Quality-control plot for the seismic inversion at the borehole sites UBGH04 (a), UBGH09 (b), and UBGH10 (c) showing a reasonably good agreement between the inverted (red line) and computed acoustic (blue line) impedance within a constraint window. For comparison, the log data are converted from depth to time. The black curves indicate the low-frequency impedance estimates extracted from the observed impedance logs (as in Fig. 10a). The red and black seismic traces are the synthetic and real seismic data, respectively. The error computation window is the time extent over which the impedance misfit was minimized during the inversion. The finer-scale details in the logs are below the resolution obtainable by the seismic data.

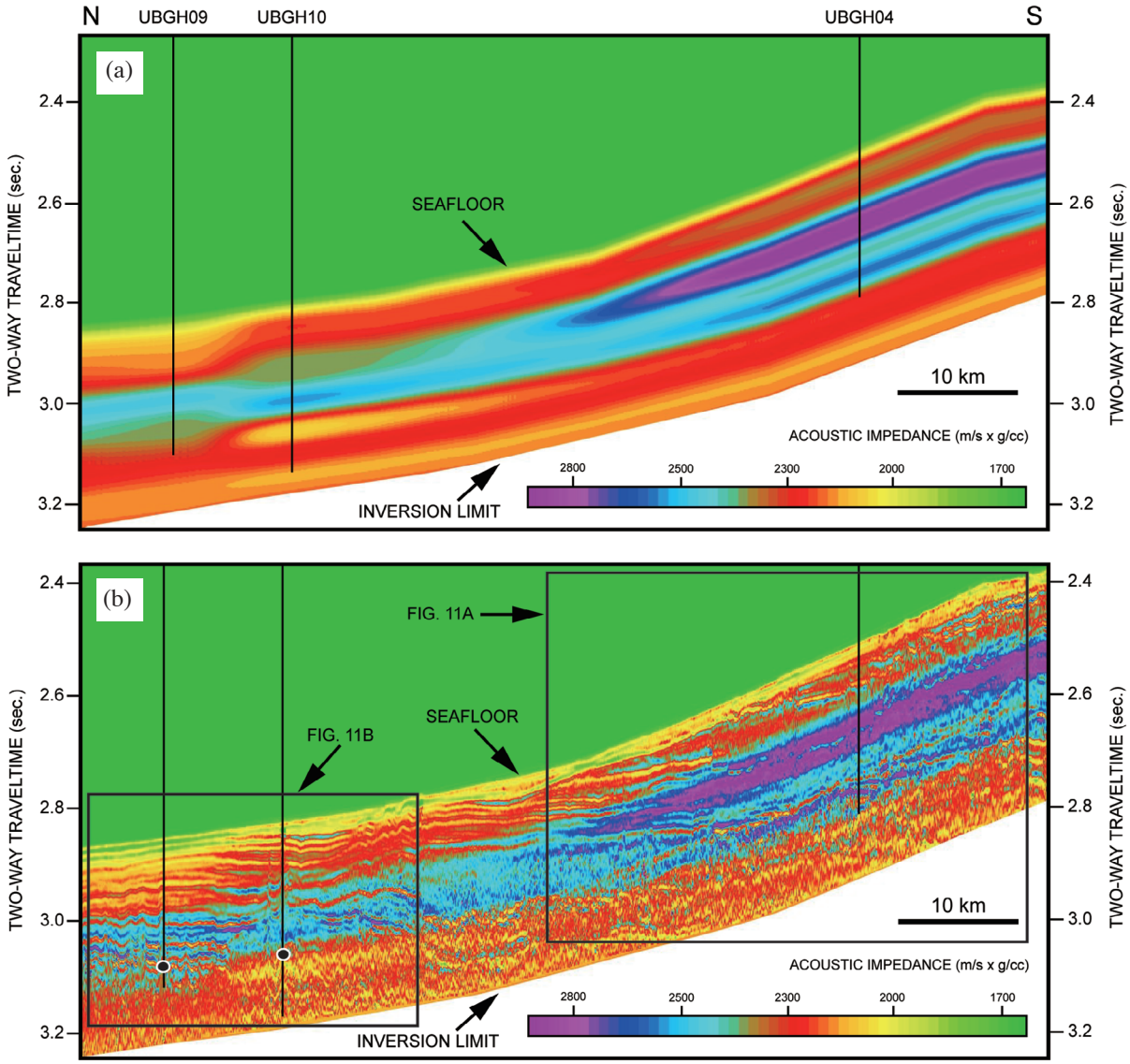

Fig. 10. (a) This low frequency background impedance model is generated from the downhole logs for the seismic inversion. This initial model is used to estimate the depths of the upper (seafloor) and lower (inversion limit) boundaries and thus to constrain the inversion. (b) Inverted seismic section with lateral variation in acoustic impedance. The steep slope shows a relatively massive (~80 ms) high-impedance zone (UIZ) under which a poorly-to-moderately continuous thin layer in the seismic impedance corresponds to the BSR; the double BSR is not defined as clearly as in Fig. 2. The gentle (lower) slope is dominated by alternating high and low impedance layers (LIZ) unless otherwise disturbed by relatively high P-wave impedance associated with either with mass-flow deposits or gas chimneys (Figs. 2 and 3).

less continuous, toward the toe of the slope but the gas hydrate stability boundary is presumed to be at about 164 (at UBGH09) to 162 (at UBGH10) mbsf as a possible bottom of the GHSZ (Table 2). In contrast, the average acoustic impedance values in the down-dip zone (LIZ in Fig. 11a) are lower than those of UIZ1 and UIZ2 in the up-dip slope area. The variation in the correlation between density and velocity at the wells (Figs. 5 and 6) is interpreted to be the result of the high degree of lithologic heterogeneity in the down-dip environment.

7.2 Interpretation

The heterogeneous high-impedance zone (LIZ in Fig. 10b) near and at UBGH09 and 10 is interpreted as a lobe of high-density, sand-rich mass-flow deposition disturbing the existing conformable layers of the THSs (Fig. 3); however, it may also be related to high-flux gas migrating through openings (Haacke et al. 2009) which we have here as evidenced by the gas chimneys (Liu and Flemings 2007). Co-existence of hydrate and gas is not unusual

in non-equilibrium conditions associated with vertical fluid transport (Zhang and McMechan 2006; Dev and McMechan 2010). Thus, the alternating higher (blue) and lower (red-yellow) impedance in the left half of Fig. 11b between 2.97 and 3.09 s, may be caused by conformably stacked turbidites characterized by graded bedding as inferred from SF2 (e.g., Ryu et al. 2009).

A thin, but discernable impedance contrast across the interpreted BSR suggests that a small amount of free gas charge may be consistently present below the GHSZ. A portion of the BSR is closely coincident with the THS scoured by the mass-transport deposits which include the site of the UBGH04. The dense (hard) mass-flow deposits underlain by the unconsolidated (soft) THS can also give a negative impedance contrast resulting in an opposite polarity at the presumed base of hydrate, compared to the seafloor (e.g., Fig. 9a). The possible BSR at UBGH04 is more likely to coincide with a vertical lithology change rather than to be an impedance contrast between hydrate and gas, or to be a combination of both. Because a lithology alternation also

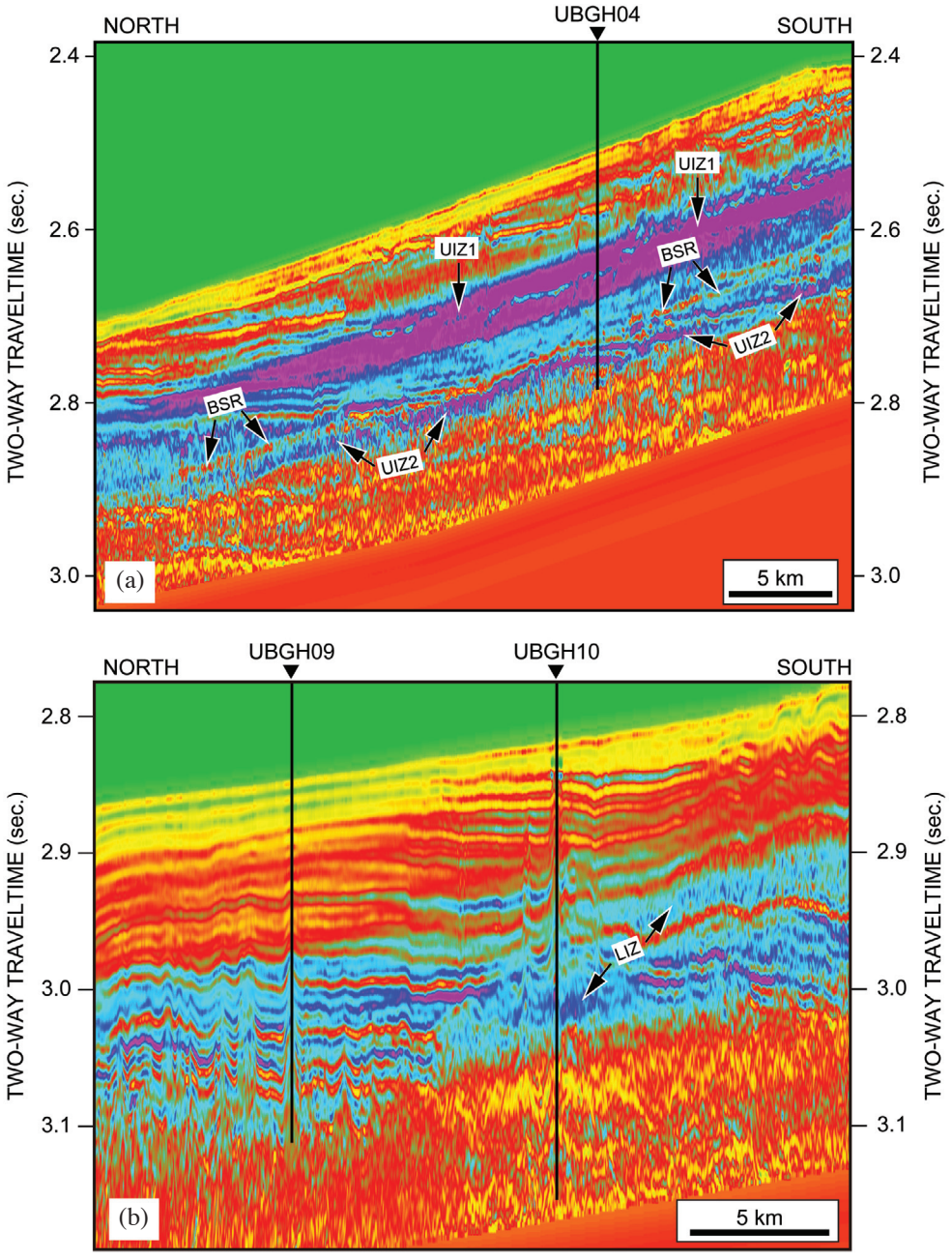

Fig. 11. Expanded view of the acoustic impedance in the up-dip slope (a) and down-dip (b) areas outlined in Fig. 10b. The black dots in the wells are at the depth of the BSR predicted from thermal calculations (Table 2). The color scale used for the impedance is the same as that in Fig. 10b.

changes the ability for hydrate to form, the bottom of the mass-transport deposits can also be coincident with the BSR in the area around the borehole. Both of these interpretations are consistent with the clearly visible BSR to either side of UBGH04 (Figs. 2 and 11a). Right at the BSR is a thin low impedance zone which is interpreted as a possible gas charge because its character is the same as the BSR in the less ambiguous parts of the section.

A possible second BSR (labeled in Fig. 2) may be associated with the presence of different gas compositions (methane, ethane, propane) that have different stability zones (Andreassen et al. 2000; Lu and McMechan 2004).

Because the neutron porosity log is available (but not shown here) it is possible to combine this with the density log to get an independent estimate of hydrate saturation/concentration (see Zhang and McMechan 2005). Water saturation (and hence hydrate or gas saturation) can also be estimated with the deviations in resistivity from the non-hydrate baseline [see, for example, Eq. (4) and Fig. 7 in Lu and McMechan 2002]. All the logs in Figs. 4, 5, and 6 show deviations (from the non-hydrated background values), in the regions that are interpreted to contain hydrates. These anomalies are consistent with the hydrate volume percent estimates from chloride concentration in Fig. 7, for wells UBGH09 and UBGH10.

The P-wave velocity at UBGH04 in the expected hydrate zone shows a positive correlation with the corresponding density log in the predicted gas hydrate stability zone (above the BSR); the density increase is interpreted to be associated with the strength and density of the debris which are caused by mass-transport flows eroding the underlying turbidites/hemipelagic sediments as indicated in the mean grain size variation. Although the impedance increase could also be the result of the presence of hydrate occurring within the mass-transport deposits, no clear evidence was found to confirm the existence of hydrates in the drilling data except at the very bottom of chlorinity and hydrate saturation logs (Fig. 7) which may also be due to data contamination while treating the core. The well log deviations for UBGH04 are not consistent with the chloride data; the letter is, however, consistent without seeing any hydrates in UBGH04. Thus, the log deviations in UBGH04 are probably caused by vertical changes in lithology rather than the presence of hydrates.

8. SUMMARY

A near-offset stacked 2D seismic reflection section is inverted to estimate the acoustic impedance of gas-and hydrate-bearing deep-water sediments in the Ulleung Basin, East Sea, Korea. Results are constrained by three LWD data suites. The inverted seismic model is derived from the near-angle stacked migrated seismic data along N-S oriented Plio-Quaternary succession containing two different facies (unconsolidated mass-flow deposits and turbidites).

A comparison of seismic reflection and computed impedance was made for two different zones: the up-dip and down-dip. The upper (steep) slope zone suggests that the BSR-like feature that was a drilling target may be caused by a local lithology boundary near the drill site of UBGH04 rather than by a phase boundary (i.e., gas below and hydrates above), but both are possible. The lower (gentle) slope zone shows that locally disturbed continuous reflections are more likely to be gas hydrate-related physical phenomena than to spatiotemporal changes in lithology.

This seismic impedance inversion enables a quantitative prediction of lithological variations which are, in turn, integrated with seismic stratigraphy and the LWD data. The integration of these differing data provides a quite informative and useful tool making a contribution to enhance interpretability of seismic profiles for gas detection and potential hydrate recovery.

Acknowledgements The authors are indebted to Dr. How-Wei Chen for providing constructive comments. This study was funded by the Gas Hydrate R/D Organization (GHDO) and Ministry of Knowledge Economy (MKE) and we also would like to thank Ministry of Land, Transport and Maritime Affairs (MLTM) for financial support for CO_2 Storage Project entitled "Construction of carbon storage map and selection of demonstration sites in Korean offshore areas." The participation of George A. McMechan was supported by the sponsors of the UT-Dallas Geophysical Consortium.

REFERENCES

Andreassen, K., J. Mienert, P. Bryn, and S. C. Singh, 2000: A double gas-hydrate related bottom simulating reflector at the Norwegian continental margin. In: Annals of the New York Academy of Sciences, vol. 912, Gas Hydrates: Challenges for the Future, 126-135, doi: 10.1111/j.1749-6632.2000.tb06766.x. [Link]

Bellefleur, G., M. Riedel, and T. Brent, 2006: Seismic characterization and continuity analysis of gas-hydrate horizons near Mallik research wells, Mackenzie Delta, Canada. *The Leading Edge*, **25**, 599-604, doi: 10.1190/1.2202663. [Link]

Buiting, J. J. M. and M. Bacon, 1999: Seismic inversion as a vehicle for integration of geophysical, geological and petrophysical information for reservoir characterization: Some North Sea examples. *Geol. Soc. Lond. Petrol. Geol.*, **5**, 1271-1280, doi: 10.1144/0051271. [Link]

CGGVeritas, 2011: STRATA, available at www.cggveritas.com/hampson-russell.aspx?cid=850&lang=1, Accessed January 1, 2011.

Dev, A. and G. A. McMechan, 2010: Interpreting structural controls on hydrate and free-gas accumulation using well and seismic information from the Gulf of Mex-

ico. *Geophysics*, **75**, B35-B46, doi: 10.1190/1.3282680. [Link]

Dickens, G. R. and M. S. Quinby-Hunt, 1997: Methane hydrate stability in pore water: A simple theoretical approach for geophysical applications. *J. Geophys. Res.*, **102**, 773-783, doi: 10.1029/96JB02941. [Link]

Fugro-McClelland, 2008: Investigation of gas hydrate expedition UBGH1, Ulleung Basin, East Sea, Offshore Korea, Field Factual Report No. 0201-6242, unpublished document.

Ginsburg, G. D., 1998: Gas hydrate accumulation in deep-water marine sediments. *Geol. Soc. Lond., Spec. Publ.*, **137**, 51-62, doi: 10.1144/GSL.SP.1998.137.01.04. [Link]

Golub, G. H. and Q. Ye, 1999: Inexact preconditioned conjugate gradient method with inner-outer iteration. *SIAM J. Sci. Comput.*, **21**, 1305-1320, doi: 10.1137/S1064827597323415. [Link]

Haacke, R. R., R. D. Hyndman, K. P. Park, D. G. Yoo, I. Stoian, and U. Schmidt, 2009: Migration and venting of deep gases into the ocean through hydrate-choked chimneys offshore Korea. *Geology*, **37**, 531-534, doi: 10.1130/G25681A.1. [Link]

Horozal, S., G. H. Lee, B. Y. Yi, D. G. Yoo, K. P. Park, H. Y. Lee, W. Kim, H. J. Kim, and K. Lee, 2009: Seismic indicators of gas hydrate and associated gas in the Ulleung Basin, East Sea (Japan Sea) and implications of heat flows derived from depths of the bottom-simulating reflector. *Mar. Geol.*, **258**, 126-138, doi: 10.1016/j.margeo.2008.12.004. [Link]

Hyndman, R. D. and E. E. Davis, 1992: A mechanism for the formation of methane hydrate and seafloor bottom-simulating reflectors by vertical fluid expulsion. *J. Geophys. Res.*, **97**, 7025-7041, doi: 10.1029/91JB03061. [Link]

Hyndman, R., G. Spence, R. Chapman, M. Riedel, and R. Edwards, 2001: Geophysical studies of marine gas hydrate in Northern Cascadia. *Geophys. Monogr. Ser.*, **124**, 273-295, doi: 10.1029/GM124p0273. [Link]

Inamori, T. and M. Hato, 2004: Detection of methane hydrate-bearing zones from seismic data. *Resour. Geol.*, **54**, 99-104, doi: 10.1111/j.1751-3928.2004.tb00191.x. [Link]

Kang, D. H., D. G. Yoo, J. J. Bahk, N. H. Koo, W. S. Kim, K. S. Park, K. P. Park, and J. S. Kim, 2009: The occurrence patterns of gas hydrate in the Ulleung Basin, East Sea. *J. Geol. Soc. Korea*, **45**, 143-155. (in Korean)

KIGAM, 2008: Analysis of gas hydrate deep-drill cores and studies on gas hydrate stability and geohazards, NP2008-003-2008, unpublished document.

Lee, H. J., S. K. Chough, and S. H. Yoon, 1996: Slope-stability change from late Pleistocene to Holocene in the Ulleung Basin, East Sea (Japan Sea). *Sediment. Geol.*, **104**, 39-51, doi: 10.1016/0037-0738(95)00119-0. [Link]

Liu, X. and P. B. Flemings, 2007: Dynamic multiphase flow model of hydrate formation in marine sediments. *J. Geophys. Res.*, **112**, B03101, doi: 10.1029/2005JB004227. [Link]

Lu, S. and G. A. McMechan, 2002: Estimation of gas hydrate and free gas saturation, concentration, and distribution from seismic data. *Geophysics*, **67**, 582-593, doi: 10.1190/1.1468619. [Link]

Lu, S. and G. A. McMechan, 2004: Elastic impedance inversion of multichannel seismic data from unconsolidated sediments containing gas hydrate and free gas. *Geophysics*, **69**, 164-179, doi: 10.1190/1.1649385. [Link]

Menke, W., 1984: Geophysical Data Analysis: Discrete Inverse Theory. Academic Press, Orlando, Florida, 260 pp.

Miles, P. R., 1995: Potential distribution of methane hydrate beneath the European continental margins. *Geophys. Res. Lett.*, **22**, 3179-3182, doi: 10.1029/95GL03013. [Link]

Netzeband, G. L., A. Krabbenhoeft, M. Zillmer, C. J. Petersen, C. Papenberg, and J. Bialas, 2010: The structures beneath submarine methane seeps: Seismic evidence from Opouawe Bank, Hikurangi Margin, New Zealand. *Mar. Geol.*, **272**, 59-70, doi: 10.1016/j.margeo.2009.07.005. [Link]

Park, K. P., J. J. Bahk, Y. Kwon, G. Y. Kim, M. Riedel, M. Holland, P. Schultheiss, K. Rose, and UBGH-1 Scientific Party, 2008: Korean national program expedition confirms rich gas hydrate deposits in the Ulleung Basin, East Sea. US Department of Energy, Office of Fossil Energy, National Energy Technology Laboratory, Spring 2008 Methane Hydrate Newsletter, 6-9.

Popescu, I., M. D. Batist, G. Lericolais, H. Nouzé, J. Poort, N. Panin, W. Versteeg, and H. Gillet, 2006: Multiple bottom-simulating reflections in the Black Sea: Potential proxies of past climate conditions. *Mar. Geol.*, **227**, 163-176, doi: 10.1016/j.margeo.2005.12.006. [Link]

Rao, Y. H., 1999: C-program for the calculation of gas hydrate stability zone thickness. *Comput. Geosci.*, **25**, 705-707, doi: 10.1016/S0098-3004(99)00012-6. [Link]

Russell, B. and D. Hampson, 1991: A comparison of post-stack seismic inversion methods. 61th Annual International Meeting, Society of Exploration Geophysicists, Expanded Abstracts, 876-878.

Ryu, B. J., M. Riedel, J. H. Kim, R. D. Hyndman, Y. J. Lee, B. H. Chung, and I. S. Kim, 2009: Gas hydrates in the western deep-water Ulleung Basin, East Sea of Korea. *Mar. Petrol. Geol.*, **26**, 1483-1498, doi: 10.1016/j.marpetgeo.2009.02.004. [Link]

Shanmugam, G., 2006: Deep-Water Processes and Facies Models: Implications for Sandstone Petroleum Reservoirs, Elsevier Science, Amsterdam, 496 pp.

Shipley, T. H., M. H. Houston, R. T. Buffler, F. J. Shaub, K. J. McMillen, J. W. Ladd, and J. L. Worzel, 1979:

Seismic evidence for widespread possible gas hydrate horizons on continental slopes and rises. *AAPG Bull.*, **63**, 2204-2213.

Shipp, C., J. A. Nott, and J. A. Newlin, 2004: Physical characteristics and impact of mass transport complexes on deepwater jetted conductors and suction anchor piles, Offshore Technology Conference, Houston, TX.

Tamaki, K. and E. Honza, 1985: Incipient subduction and deduction along the eastern margin of the Japan Sea. *Tectonophysics*, **119**, 381-406, doi: 10.1016/0040-1951(85)90047-2. [Link]

Tamaki, K., K. Suyehiro, J. Allan, J. C. Ingle, and K. A. Pisciotto, 1992: Tectonic synthesis and implications of Japan Sea ODP drilling. Proceedings of the Ocean Drilling Program, Scientific Results, vol. 127/128, Part 2, 1333-1348.

Veeken, P. C. H. and M. D. Silva, 2004: Seismic inversion methods and some of their constraints. *First Break*, **22**, 47-70, doi: 10.3997/1365-2397.2004011. [Link]

Wood, W. T., J. F. Gettrust, N. R. Chapman, G. D. Spence, and R. D. Hyndman, 2002: Decreased stability of methane hydrates in marine sediments owing to phase-boundary roughness. *Nature*, **420**, 656-660, doi: 10.1038/nature01263. [Link]

Yoon, S. H., S. K. Chough, and S. J. Park, 2003: Sequence model and its application to a Miocene shelf-slope system in the tectonically active Ulleung Basin margin, East Sea (Sea of Japan). *Mar. Petrol. Geol.*, **20**, 1089-1103, doi: 10.1016/j.marpetgeo.2003.08.001. [Link]

Zhang, Z., and G. A. McMechan, 2006: Elastic inversion for distribution of gas hydrate, with emphasis on structural controls. *J. Seism. Explor.*, **14**, 349-370.